Atmospheric
Chemistry
and Physics

Open Access

Discussions

Aerosol optical properties in the southeastern United States in summer – Part 1: Hygroscopic growth

C. A. Brock[1], N. L. Wagner[1,2], B. E. Anderson[3], A. R. Attwood[1,2,a], A. Beyersdorf[3], P. Campuzano-Jost[2,4], A. G. Carlton[5], D. A. Day[2,4], G. S. Diskin[a], T. D. Gordon[1,2], J. L. Jimenez[2,4], D. A. Lack[1,2,b], J. Liao[1,2], M. Z. Markovic[1,2,c], A. M. Middlebrook[1], N. L. Ng[6,7], A. E. Perring[1,2], M. S. Richardson[1,2], J. P. Schwarz[1], R. A. Washenfelder[1,2], A. Welti[1,2,d], L. Xu[6], L. D. Ziemba[3], and D. M. Murphy[1]

[1]NOAA Earth System Research Laboratory, Boulder, CO, USA
[2]Cooperative Institute for Research in Environmental Sciences, University of Colorado, Boulder, CO, USA
[3]NASA Langley Research Center, Hampton, VA, USA
[4]Department of Chemistry and Biochemistry, University of Colorado, Boulder, CO, USA
[5]Department of Environmental Sciences, Rutgers University, New Brunswick, NJ, USA
[6]School of Earth and Atmospheric Sciences, Georgia Institute of Technology, Atlanta, GA, USA
[7]School of Chemical and Biomolecular Engineering, Georgia Institute of Technology, Atlanta, GA, USA

Discussion Paper | Discussion Paper | Discussion Paper | Discussion Paper

ACPD

15, 25695–25738, 2015

Aerosol hygroscopicity in the southeastern US

C. A. Brock et al.

Title Page

Abstract | Introduction

Conclusions | References

Tables | Figures

◄ | ►

◄ | ►

Back | Close

Full Screen / Esc

Printer-friendly Version

Interactive Discussion

[a]now at: Horiba Scientific, Edison, NJ, USA
[b]now at: TEAC Consulting, Brisbane, Australia
[c]now at: Air Quality Research Division, Environment Canada, Toronto, Ontario, Canada
[d]now at: Leibniz Institute for Tropospheric Research, Department of Physics, Leipzig, Germany

Correspondence to: C. A. Brock (charles.a.brock@noaa.gov)

Full Screen / Esc

Printer-friendly Version

Interactive Discussion

Abstract

Aircraft observations of meteorological, trace gas, and aerosol properties were made during May–September 2013 in the southeastern United States (US) under fair-weather, afternoon conditions with well-defined planetary boundary layer structure. Optical extinction at 532 nm was directly measured at three relative humidities and compared with extinction calculated from measurements of aerosol composition and size distribution using the κ-Köhler approximation for hygroscopic growth. Using this approach, the hygroscopicity parameter κ for the organic fraction of the aerosol must have been < 0.10 to be consistent with 75 % of the observations within uncertainties. This subsaturated κ value for the organic aerosol in the southeastern US is consistent with several field studies in rural environments.

We present a new parameterization of the change in aerosol extinction as a function of relative humidity that better describes the observations than does the widely used power-law (gamma, γ) parameterization. This new single-parameter κ_{ext} formulation is based upon κ-Köhler and Mie theories and relies upon the well-known approximately linear relationship between particle volume (or mass) and optical extinction (Charlson et al., 1967). The fitted parameter, κ_{ext}, is nonlinearly related to the chemically derived κ parameter used in κ-Köhler theory. The values of κ_{ext} we determined from airborne measurements are consistent with independent observations at a nearby ground site.

1   Introduction

Particles in the atmosphere scatter and absorb solar radiation. Atmospheric aerosol extinction (= scattering + absorption) reduces visibility and usually cools the earth, especially over dark surfaces such as oceans and forests. Uncertainty in the direct climate forcing due to anthropogenic aerosols is the second largest contributor to total uncertainty in climate forcing (IPCC, 2013).

One of the most important factors affecting ambient aerosol optical extinction – hence visibility, aerosol optical depth (AOD), and direct radiative effects – is the particulate water mass, which depends on both the hydrophilic properties of the aerosol components and the relative humidity (RH). Hygroscopic water uptake changes particle size and refractive index and can lead to dramatic changes in the extinction as a function of RH due to changes in the amount of aerosol liquid water, even when dry mass is constant. Since atmospheric RH is highly variable temporally, horizontally, and especially vertically, aerosol water plays an important role in the relationship between ambient extinction and dry aerosol mass.

The relationship between atmospheric extinction and humidity has long been recognized (e.g., Wright, 1939). The coupling between particle hygroscopicity and composition and optical extinction has been evaluated experimentally and quantitatively since the work of Pilat and Charlson (1966), Covert and Charlson (1972) and Hänel (1972a, 1972b). Because of the chemical complexity of particles and the difficulty in measuring their molecular composition and relating that to water uptake with increasing RH, it is common to use simplified parameterizations to describe the change in extinction (or scattering) with atmospheric RH relative to a dry or low-RH state. The most frequently used of these parameterizations is a power-law function known as the "gamma" parameterization, which was first used by Kasten et al. (1969). This empirically derived, single parameter equation is often written as

$$\frac{\sigma(\mathrm{RH})}{\sigma(\mathrm{RH}_0)} \equiv f(\mathrm{RH}) = \left[\frac{(100 - \mathrm{RH}_0)}{(100 - \mathrm{RH})}\right]^{\gamma}, \tag{1}$$

where $\sigma(\mathrm{RH})$ is the bulk aerosol extinction at the ambient RH condition, $\sigma(\mathrm{RH}_0)$ the extinction at the dry (low RH) condition RH_0, and γ is a parameter fitted to the observed data. The γ parameterization has been widely used to describe aerosol hygroscopicity (e.g., Attwood et al., 2014; Doherty et al., 2005; Kasten, 1969; Massoli et al., 2009; Quinn et al., 2005). Doherty et al. (2005) and Quinn et al. (2005) showed that in many environments the value of γ varies systematically with composition, and especially with

the ratio of submicron organic aerosol (OA) mass to the mass of submicron sulfate plus OA. Thus one can approximately predict f(RH) at arbitrary RH given information on bulk submicron particle composition.

In this paper we examine the change in aerosol extinction at 532 nm wavelength as a function of RH based on measurements from two airborne field projects in the southeastern US in the summer. This analysis focuses on mid-day and afternoon data collected when the planetary boundary layer was fully developed because (1) prior to daytime atmospheric mixing, aerosols may be chemically diverse and externally mixed, leading to complex hygroscopic growth patterns that are hard to characterize (Santarpia, 2005), (2) we wish to develop an understanding of aerosol hygroscopicity that is regionally representative, and the well-developed, cloud-topped boundary layer structure examined here is typical of the southeastern US in summertime (Warren et al., 1986); and (3) most of the airborne data were taken in the late morning and afternoon in fair weather. By applying κ-Köhler and Mie theories to these data, we develop a new single-parameter equation to accurately describe f(RH). The relationship between this new parameter, κ_{ext}, and the hygroscopicity parameter κ from κ-Köhler theory is examined, and the new parameterization is compared to the γ power-law model.

In a companion paper (Brock et al., 2015; hereafter Part 2), the understanding of aerosol hygroscopicity developed here and the same data are used to evaluate the sensitivity of AOD to a range of aerosol and meteorological parameters. Part 2 also contains details of the selection of data for the analyses in both papers and the development of representative profiles for calculation of AOD sensitivities.

2 Methods

2.1 Aircraft instrumentation

We analyze airborne, in situ data measured during vertical profiles from the May–July 2013 Southeastern Nexus of Air Quality and Climate (SENEX) and the portions

Aerosol hygroscopicity in the southeastern US

C. A. Brock et al.

of the August–September 2013 Study of Emissions and Atmospheric Composition, Clouds, and Climate Coupling by Regional Surveys (SEAC[4]RS) projects that were made in the southeastern US. The SENEX project used the NOAA WP-3D aircraft (typical airspeed $\sim 100\,\mathrm{m\,s^{-1}}$), while the SEAC[4]RS project used the NASA DC-8 air-craft ($\sim 160\,\mathrm{m\,s^{-1}}$) Details of the instruments, measurements, and methodology for generating regionally representative vertical profiles of aerosol, gas-phase, and me-teorological parameters are given by Wagner et al. (2015). Briefly, measurements of the composition of sub-1 µm vacuum aerodynamic diameter (approximately < 0.7 µm physical diameter) non-refractory particles were made by aerosol mass spectrome-ters (AMS, Aerodyne, Billerica, Massachusetts, USA; Canagaratna et al., 2007; De-Carlo et al., 2006) each with extensive customization for aircraft use (Bahreini et al., 2008; Dunlea et al., 2009; Middlebrook et al., 2012). The AMS used during SENEX employed a compact time-of-flight mass spectrometer (CTOF) while that used during SEAC4RS employed a high-resolution time-of-flight mass spectrometer with greater re-solving power (HRTOF, DeCarlo et al., 2006). The mass of black carbon (BC) particles was measured on both projects with the same humidified tandem single-particle soot photometer (SP2; Droplet Measurement Technologies, Boulder, CO, USA; Schwarz et al., 2015). Dry particle size distributions from ~ 0.07 to 1.0 µm were measured with two separate ultra-high sensitivity aerosol size spectrometers (UHSAS, Particle Met-rics, Inc., Boulder, Colorado, US; Brock et al., 2011; Cai et al., 2008), one on each project. Aerosol extinction at 532 nm wavelength and three relative humidities (~ 15, ~ 70, and ~ 90 %) was measured simultaneously with a custom built multichannel cav-ity ringdown spectrometer (CRDS; Langridge et al., 2011) on both projects.

Air entering the CRDS passed through a 40 cm long carbon monolith denuder (210 cpi 30 mm^{-1} OD, MAST Carbon, Basingstoke, UK) to remove semivolatile inor-ganic and organic gases. The flow was then was dried to a low RH (usually < 15 % and always < 25 %, below the efflorescence point of atmospherically relevant salts) using multitube Nafion dryers (PD-200T-12MSS, Permapure Inc., Toms River, New Jersey, US) with a sample residence time of 0.25 s. For measurement by the two elevated

Discussion Paper | Discussion Paper | Discussion Paper | Discussion Paper | Discussion Paper |

Title Page

Abstract   Introduction

Conclusions   References

Tables   Figures

◄   ►

◄   ►

Back   Close

Full Screen / Esc

Printer-friendly Version

Interactive Discussion

RH channels, the sample was humidified to $> 90\%$ RH by cooling the sample flow inside Nafion humidifiers (MH-110-12-S-4, Permapure Inc., Toms River, New Jersey, US), causing deliquescence. The sample flow was then reheated to the temperature of the measurement cells in the instrument, which were controlled using RH sensors (Model HMP110, Vaisala Inc., Helsinki, Finland) to achieve the desired measurement RH. Typically, one channel measured at $\sim 70\%$ RH and the other measured at $\sim 90\%$ RH. The cooling in the humidifiers was 10–15 and 1–3 K below the cell temperatures of the medium- and high-RH channels respectively. Total time of exposure to elevated humidities was $\sim 4\,\mathrm{s}$, of which $0.4\,\mathrm{s}$ was in the cooled section and $3.6\,\mathrm{s}$ was in the warmed section. Calculated and measured $f(\mathrm{RH})$ for 300 nm ammonium sulfate particles are in agreement within uncertainties (Langridge et al., 2011), indicating that the humidified residence time is sufficient to allow hygroscopic particles to grow to equilibrium. However, the instrument has not been tested with less hygroscopic organic particles that might exhibit kinetic limitations to water uptake. This remains an uncharacterized uncertainty. The changes in sample temperature in the inlet, sample line, humidifiers, and CRDS cells may lead to loss of semi-volatile species; these possible effects are ignored. Condensation of semi-volatile compounds is excluded by the upstream denuder. Because of the initial high level of humidification prior to reheating, the CRDS measurements at elevated RH were made on the metastable (humidified) branch of any deliquescence/efflorescence hysteresis curve. This better represents the likely state of the aged atmospheric aerosol in the cloud-topped planetary boundary layer than would measurements made on the deliquescence branch of the curve. We did not attempt to measure aerosol extinction at ambient humidity because it is difficult to regulate instrument humidity rapidly enough to respond to ambient RH changes in flight.

The CRDS optical extinction measurements were made behind an impactor with a 50% efficiency at $1.0\,\mu\mathrm{m}$ aerodynamic diameter. Accounting for particle and air density, typical 50% impactor efficiency was $\sim 0.7\,\mu\mathrm{m}$ physical diameter at the inlet RH, which was measured at $< 50\%$ during SENEX due to dynamic heating dur-

ing sampling, and was presumably lower during SEAC[4]RS due to the higher aircraft speed. Coarse (> 0.7µm) particle size distributions were measured during SENEX with a custom-built white-light optical particle counter at < 50 % RH conditions (Brock et al., 2011), allowing calculation of coarse particle extinction. The contribution to extinction due to dry coarse particles was estimated using Mie theory and an assumed refractive index of $1.59 + 0i$ (that of the polystyrene latex (PSL) sphere calibrant), and was on average < 7 % of the total calculated extinction for the data measured in the planetary boundary layer. We ignore the contribution to extinction for particles larger than 0.7 µm physical diameter in the remainder of this work. Based on the known particle transmission characteristics of the AMS inlet and the measured size distribution, the AMS was estimated to sample > 97 % of the sub-0.7 µm particle volume (Wagner et al., 2015); the AMS, CRDS, SP2, and UHSAS all comparably and quantitatively sampled the sub-0.7 µm aerosol.

2.2 Corrections to UHSAS size distributions for refractive index

The size distribution reported by the UHSAS is a function of the amount of light scattered onto the instrument's photodetectors, and the quantity of scattered light is itself a function of the composition-dependent aerosol refractive index. Hence, it is necessary to correct the measured UHSAS size distributions for changing aerosol composition during flight. This correction was accomplished by first calibrating the instrument to an aerosol of known refractive index to relate scattering amplitude to discrete pulse height channels. Next, the Mie scattering over the optical geometry of the instrument was calculated to determine how each channel was related to particle diameter for an atmospherically relevant range of real refractive index. Finally, a look-up table of this relationship was used to determine the actual diameter represented by each channel as refractive index, calculated from the AMS measurements as described in Sect. 2.3, varied.

The UHSAS operated during SENEX was calibrated using atomized, dried ammonium sulfate particles sized with a custom-built differential mobility analyzer (DMA) of a design now available commercially (Brechtel Manufacturing, Inc., Hayward, CA, US). The sizing accuracy of the DMA was better than 2 % as determined using NIST-traceable PSL microspheres in eight sizes from 0.1 to 1.2 µm (Thermo Fisher Scientific, Inc., Waltham, MA, US). The UHSAS was calibrated on five days with > 36 separate ammonium sulfate particle sizes during the SENEX mission, in addition to pre-flight daily calibration checks using four PSL microsphere sizes. The UHSAS that was operated by the NASA Langley group during SEAC[4]RS was calibrated using PSL microspheres and the calibration was checked twice during each flight by generating an aerosol containing four microsphere sizes and introducing it into the inlet sample flow as the aircraft was flying.

The response of the UHSAS was simulated using numerical Mie calculations (Bohren and Huffman, 1983) of the light scattered over the solid angle that is imaged onto the instrument's photodetectors. Assumptions include spherical, homogeneous particles with composition that is invariant with particle diameter. The geometry of the detection optics was determined from a review of technical drawings with the manufacturer. Light is scattered perpendicularly to the beam from a neodymium-doped yttrium lithium fluoride laser (1053 nm) and is imaged onto solid state photodetectors on each side of the scattering cell using pairs of Mangin mirrors in clamshell configurations. The signal from each detector is amplified through two gain stages, for a total of four independent gain stages. Each detector samples the light scattered by particles over a circularly symmetric angle from 33–147°. The center region of the angle, between 75.2 and 104.8° is not sampled because the hole cut in the outer of the Mangin mirrors (the detector area is a negligible fraction of this hole area). Thus the imaged solid angle is a conical annulus. This geometry contrasts with that reported for the UHSAS by Cai et al. (2008), who appear to have incorrectly used a 22–158° scattering angle to simulate UHSAS instrument response, but is consistent with that reported by Petzold et al. (2013).

Using the calibrations, the relationship between the 99 size channels and the amount of light scattered onto the detectors was determined. Knowing that each channel represents a certain amount of scattered light, the Mie model was used to calculate the particle diameter corresponding to each channel for a range of particle real refractive indices from 1.40 to 1.60, in increments of 0.01, producing a look-up table relating channel number to particle diameter as a function of real refractive index. Using the AMS data and the composition model described in Sect. 2.3, the real refractive index was determined by volume-weighted averaging for each AMS data point using the values in Table 1. The mean and standard deviation of the real part of the calculated refractive index was 1.547 ± 0.004 for the data analyzed here. Using the real refractive index for each point, the look-up table was then applied to determine the physical diameter for each UHSAS channel for each measurement interval. Residual water content in the dry ($< 25\%$ RH) aerosol was not considered. The variation in instrument response due to the imaginary component of the refractive index, k, also was not considered. Because BC concentrations were very low (averaging $< 0.05\,\mu g\,m^{-3}$ for the data analyzed here), k was calculated to be 0.006 ± 0.004, and thus was ignored in the generation of the UHSAS look-up table. However, the BC component was included in the calculation of κ_{chem}, refractive index, and extinction as described in Sect. 2.3 below.

2.3 Method to calculate ambient extinction

To determine ambient extinction, measurements of extinction made at three discrete RH values of < 15, ~ 70, and $\sim 90\%$ may be interpolated or extrapolated to ambient conditions at arbitrary RH based on a parametric model such as the γ function. However, because the measurements analyzed here include submicron aerosol size distributions and composition, a more explicit and accurate method to determine ambient extinction can also be used (Fig. 1a). Petters and Kreidenweis (2007) proposed the κ-Köhler parameterization that describes the water activity of an aqueous solution without considering explicitly the effect of individual ionic components. The κ-Köhler approach has been used widely to predict subsaturated particle growth as well as the

activation of cloud condensation nuclei. Ignoring curvature effects for particle diameters > 100 nm, the hygroscopic growth of a water-soluble aerosol can be approximated as

$$\mathrm{gf_{diam}} \cong \left(1 + \kappa_{chem}\frac{RH}{100 - RH}\right)^{1/3}, \tag{2}$$

5 where $\mathrm{gf_{diam}}$ is the diameter growth factor, the ratio of the particle's wet diameter to its dry diameter. An equation of this form was first used by Rissler et al. (2006) to describe observed hygroscopic growth factors. The parameter κ_{chem} may be calculated from the volume-weighted contribution due to species i, κ_i, which are determined from thermodynamic model calculations or by experimentally determining the growth factors
10 for individual compounds, as

$$\kappa_{chem} = \frac{\sum_i (\kappa_i X_i/\rho_i)}{\sum_i (X_i/\rho_i)}, \tag{3}$$

where X_i is the mass concentration and ρ_i the dry density of species i. This volume-weighted approach follows the Zdanovskii–Stokes–Robinson (Stokes and Robinson, 1966) mixing rule, which states that each component of the mixture acts independently and that the optical properties are linearly additive. The accuracy of the particle diam-
15 eter growth factor calculated using κ_{chem} determined from Eq. (3) varies depending on the specifics of the aerosol composition and mixing state and on the accuracy of the κ_i, but is generally observed to be better than 30 % (Petters and Kreidenweis, 2007).

Using the methodology shown schematically in Fig. 1a, the measurements of aerosol
20 composition and size distribution were used to calculate the extinction expected at the dry, medium, and high RH values measured in the CRDS. This calculation serves two purposes: it evaluates the closure of the optical, chemical, and size distribution measurements, and it helps evaluate how well the γ parameterization, Eq. (1), describes

Aerosol hygroscopicity in the southeastern US

C. A. Brock et al.

f(RH) in the southeastern US. The AMS measured the mass concentrations of sulfate, nitrate, chloride, ammonium, and OA. From these measurements, an electrolyte composition model (Zaveri, 2005) was used to calculate the concentrations of ammonium sulfate, ammonium bisulfate, letovicite, sulfuric acid, ammonium nitrate, ammonium
5   chloride, nitric acid, and hydrochloric acid. Contributions from ions associated with electrolytes of magnesium and sodium are likely to be insignificant contributors to the submicron aerosol mass in the continental boundary layer (Washenfelder et al., 2015). Organosulfates were estimated to contribute < 4 % to the submicron aerosol mass and therefore are not considered (Liao et al., 2015). The contribution of particulate organic
10 nitrates (pON) to measured nitrate has been estimated using the method described in Fry et al. (2013) for the SEAC[4]RS flights on which the HRTOF-AMS was operated (Day et al., 2015). The pON, likely in the form of oxidized monoterpene nitrates (Boyd et al., 2015; Draper et al., 2015; Xu et al., 2015a) is estimated to be between 15 and 40 % of the total measured nitrate above the surface in the well-mixed and transition layers,
15 and more than 63 % across the southeastern US at the surface (Xu et al., 2015a). However, nitrate represented < 5 % of fine aerosol mass in the data analyzed here. Lacking specific information on pON density or hygroscopicity, and given its small contribution to aerosol mass (< 12 % of OA and < 8 % of submicron mass; Xu et al., 2015b), all measured nitrate is treated as ammonium nitrate. Finally, potential phase separation
20 phenomena that have been found in laboratory studies of OA/inorganic mixtures (e.g., Hodas et al., 2015), insoluble inclusions that might influence hygroscopicity (Pringle et al., 2010), and the diameter dependence of κ_{chem} discussed by Good et al. (2010a) are ignored.

The bulk aerosol κ_{chem} was determined from the volume-weighted κ_i values (Table 1)
25 using Eq. (3). Aerosol extinction at the measured low, medium and high humidities was then calculated as follows (Fig. 1a). First, as detailed in Sect. 2.2., the optically equivalent dry diameters measured by the UHSAS were converted into physical dry diameters, accounting for the effects of varying composition on the real refractive index, which varied only slightly (interdecile range 1.54–1.56). Next, the particle diameter at

Aerosol hygroscopicity in the southeastern US

C. A. Brock et al.

Title Page

Abstract	Introduction
Conclusions	References
Tables	Figures

Back | Close

Full Screen / Esc

Printer-friendly Version

Interactive Discussion

the ambient RH, D_{RH}, was calculated using κ-Köhler theory (including the Kelvin effect) by numerically solving

$$\frac{RH}{100} = \frac{D_{RH}^3 - D_d^3}{D_{RH}^3 - D_d^3(1 - \kappa_{chem})} \exp\left(\frac{4\sigma_s M_w}{RT\rho_w D_{RH}}\right) \tag{4}$$

where D_d is the dry diameter, σ_s the surface tension of water at the particle/air interface, and M_w and ρ_w the molecular weight and density of water, respectively (Petters and Kreidenweis, 2007). Finally, Mie theory (Bohren and Huffman, 1983) was used to calculate the expected extinction coefficient, σ_{ext}, at the ambient RH using the water-swelled D_{RH} and water-corrected, volume-weighted refractive index n, as

$$\sigma_{ext} = \int_{4\,nm}^{700\,nm} \frac{\pi}{4} D_{RH}^2 \alpha(D_{RH}, n) N(D_{RH}) dD_{RH}, \tag{5}$$

where α is the extinction efficiency and N the number concentration of particles in diameter interval dD_{RH}.

In calculating ambient extinction using Eq. (5) it is assumed that there is no size dependence to κ_{chem}; instead it is assumed that all optically active particles are spherical, internally mixed and have the same composition regardless of size. This assumption is supported qualitatively by inspection of the size-dependent composition periodically measured by the AMS instruments. The differences in the real refractive index between the UHSAS sensing laser (1053 nm) and the humidified CRDS (532 nm) wavelengths of about 0.02 (Toon et al., 1976) are not considered. We also ignore the contribution of submicron soil components, which were not separately measured but whose concentrations measured at a surface site nearby were negligible (Washenfelder et al., 2015), and of sea-salt.

2.4 Uncertainty in calculated and measured extinction

Extinctions were calculated from the measured composition and the UHSAS size distributions for the low (< 25 % RH) medium (~ 70 % RH) and high (~ 90 % RH) conditions of measurement in the CRDS instrument. The uncertainties in these extinctions are difficult to estimate because of the multiple steps of processing (Fig. 1a), including modeling the UHSAS instrument response, and the assumptions inherent in the calculation (e.g., internally mixed, homogeneous, spherical particles). We assume that κ_{chem} for inorganic electrolytes can be estimated to within ~ 20 %, based on ranges found in the cited literature. This uncertainty includes the uncertainty in the composition determined by the AMS. This uncertainty may appear low, since AMS accuracy for absolute concentrations is ~ 35 %, driven in large part by uncertainties in particle collection efficiency (Middlebrook et al., 2012). However, only the mass fractions of the individual aerosol constituents are used when calculating κ_{chem}, so the collection efficiency does not contribute to the uncertainty assuming that all components of a particle are collected with the same efficiency. Instead, the uncertainty is dominated by other factors such as relative ionization efficiency for different compounds, and is taken to be ~ 20 %; this uncertainty is an area of current research. For OA, the uncertainty in the κ_{chem} is much larger because the OA composition is largely unknown. Values of κ_{chem} for various OA compositions measured in the laboratory vary from 0 to 0.5 (e.g., Petters and Kreidenweis, 2007; Rickards et al., 2013). To achieve consistency with the observed $f(\mathrm{RH})$, we have chosen a κ_{chem} for OA, $\kappa_{chem,\,org}$, of 0.076. The range of $\kappa_{chem,\,org}$ values that are consistent with our observations within uncertainties is discussed further in Sect. 3.1.

The uncertainty in the size distribution measured by the UHSAS has been examined in detail elsewhere (see Supplement in Brock et al., 2011). For particle diameters < 0.5 µm, and an assumed range in real refractive index of 1.43–1.56 with negligible absorption, the actual diameter may deviate by up to 8 % from the reported diameter, which is based on ammonium sulfate calibration. However, because we correct the

size distribution for refractive index effects as described in Sect. 2.2, the error in the diameters used to calculate extinction is estimated to be $< 3\%$ based on calibration precision. Concentration uncertainty due to counting statistics is $< 4\%$ for the cases analyzed here, and that due to the sample flow measurement is $< 1.6\%$. The absolute uncertainty in the measurement of the instrumental RH is $\pm 2\%$, increasing to $\pm 3\%$ for RH values exceeding 90 %.

The uncertainties described above propagate to extinction nonlinearly through the κ-Köhler equation (Eq. 4) and through the Mie calculation (Eq. 5). We use a Monte Carlo approach to simulate the expected uncertainty in the extinction determined at the three relative humidities. Three values each of geometric mean diameter, geometric standard deviation, and κ_{chem} were chosen spanning the interdecile range of observed values, creating a total of 27 cases. For each case, the extinction at the three RH values was calculated, as described in Sect. 2.3 (Fig. 1a), 1000 times while median diameter, standard deviation, κ_{chem}, and RH each was simultaneously varied by a normally-distributed random error corresponding to the uncertainty in that parameter. In addition, a normally-distributed random uncertainty was added to represent counting statistics and flow uncertainty. The resulting total relative errors for calculated extinction varied only slightly as function of extinction, with a mean relative error of $\pm 34\%$. This value is used as the best estimate of total uncertainty in calculated ambient extinction.

The calibration accuracy in directly-measured CRDS extinction varies with measurement RH, and is $\pm 2\%$ at $< 25\%$ RH, $\pm 5\%$ at 70 % RH, and $\pm 15\%$ at 90 % RH for extinction values exceeding $20\,\mathrm{M\,m^{-1}}$. Instrument precision for 1 s data is $\pm 5\%$ at $50\,\mathrm{M\,m^{-1}}$.

For the seven flights analyzed for this study, the extinction calculated from the AMS and size distribution data (Sect. 2.3) and the extinction measured by the CRDS agreed within the combined experimental uncertainty at all three measurement humidities (Table 2, Fig. 2). During the SEAC4RS flight of 6 September 2013, the UHSAS did not function, so data from a laser aerosol spectrometer (LAS, TSI, Inc., St. Paul, MN, US) were used for the size distributions instead. We do not have an instrument model with

which to correct the reported LAS size distribution, calibrated using PSL microspheres, for refractive index effects. The calculated low-RH extinction values for this flight were 38 % lower than the measured values. However, the calculated and measured f(RH) showed no substantial bias for this flight, which suggests a LAS concentration error rather than a bias in measured particle diameter. Because this flight was one of only two from late summer contributing to the analyzed dataset, to improve seasonal representativeness the data from this flight are included in the analysis despite the differences in instrumentation.

3   Results and analysis

The optical extinction of summertime, daytime aerosol in the cloud-topped boundary layer of the southeastern US was measured at three RH values (Fig. 2). At the medium (∼ 70 %) RH, the optical extinction was higher than the low-RH extinction by a factor of only ∼ 1 to 1.5. At the high (∼ 90 %) RH, the aerosol displayed a much wider range of f(RH) values, varying from 1.2 to 3.5, with a modal value of ∼ 1.8 (Fig. 3). For comparison, the f(RH) for pure 300 nm ammonium sulfate particles at 532 nm wavelength is expected to be ∼ 2 at 70 % RH and ∼ 4 at 90 % RH (Langridge et al., 2011). In the following sections we develop a new parameterization to describe the f(RH) curve, explore the relationship between particle composition and this parameterization, and place constraints on the hygroscopicity of the OA component of the submicron aerosol.

3.1   Parameterizing f(RH)

The hygroscopic growth of particles and f(RH) can be calculated using the technique shown in Fig. 1a. However, a simplified parameterization based on optical measurements alone (Fig. 1b) is useful when compositional or size distribution observations are not available. The often-used γ parameterization (Eq. 1) has the desired simplicity; however, as shown in Fig. 4a, it does not produce a hygroscopic growth curve

that matches the f(RH) directly observed or calculated from the composition and size distribution measurements used in this analysis. Values of γ fitted to the f(RH) data (Fig. 4a), overpredict observed f(RH) at 70 % RH. The planetary boundary layer in the southeastern US is often at humidities between 50 and 90 % where the γ parameterization could lead to overprediction of the ambient extinction by 20 % or more. Because of these biases we have sought a different single-parameter representation of the f(RH) curve.

We use κ-Köhler theory to develop an alternative parameterization for f(RH). The cube of the diameter growth factor gf_{diam} (Eq. 2) is the volume growth factor. Relating the volume growth factor to bulk f(RH) however, involves the complicated variation of aerosol extinction efficiency as a function of particle diameter, often described using Mie theory. As particles grow due to water uptake as RH increases, the extinction cross section can change non-linearly, and can even decrease (e.g., Bohren and Huffman, 1983). However, as pointed out earlier (Chylek, 1978; Pinnick et al., 1980), for a physically realistic, polydisperse aerosol composed of particles predominantly smaller than the wavelength of light (but larger than Rayleigh scatterers), σ_{ext} is roughly proportional to integrated particle volume or mass. This proportionality results because the extinction efficiency $\alpha(D_p, n)$ for visible light can be approximated as a linear function of particle diameter over the relatively broad size range of a polydisperse accumulation mode atmospheric aerosol (i.e., α is proportional to D_p, Fig. 5). If this is true, it follows from Eq. (5) that $\sigma_{ext} \propto D_p^3$: extinction is proportional to volume. Thus the relative change in extinction, f(RH), is roughly proportional to the relative change in volume, which for the case of a deliquescing aerosol is the volume growth factor gf_{vol}. This proportionality applies for an aerosol of constant refractive index, which is not the case for an atmospheric aerosol particle growing by addition of water with increasing RH (Hänel, 1976; Hegg et al., 1993). This $\sim$ 20 % effect on f(RH) due to refractive index change for RH ≤ 90 % (Hegg et al., 1993) can be ignored to first order. The approximate proportionality between extinction and volume is valid for particles smaller than the wavelength of light, which for these measurements is 532 nm. The 10th to 90th per-

centile range for the geometric median diameters considered here was 120–170 nm, so this approximation is valid, even for particles at high RH. The approximate (no Kelvin effect) diameter growth factor from κ-Köhler theory is given in Eq. (2). The cube of this this is then roughly proportional to gf_{vol} and $f(RH)$:

$$gf_{vol} \propto f(RH) \cong 1 + \kappa_{ext} \frac{RH}{100 - RH}, \tag{6}$$

where κ_{ext} is a dimensionless parameter fitted to observed $f(RH)$. When fitted to the three-point $f(RH)$ measurements in SENEX and SEAC^{4}RS, both the κ_{ext} and γ parameterizations describe the high RH condition well (Fig. 4a). However, the κ_{ext} parameterization predicts the medium-RH extinction values better than does the γ parameterization. This improved performance is shown Fig. 4b, where the fitted and measured $f(RH)$ values at the medium (70%) RH condition for the two parameterizations are compared. The ratio of fitted to measured medium-RH $f(RH)$ values for κ_{ext} is centered near 1 and is symmetric, while that for γ is > 1. Further, there are distinct differences in the fitted $f(RH)$ curves for the two approaches for RH > 90%, with the κ_{ext} parameterization showing a more rapid increase in $f(RH)$ with increasing RH for these high humidity conditions. Preliminary evaluation of ambient atmospheric data acquired in winter 2015 in Boulder, Colorado, US (not shown) confirms that the κ_{ext} curve more closely follows the observed $f(RH)$ for ambient particles at RH > 90% than does the γ parameterization.

In summary, the power-law γ parameterization for $f(RH)$ did not adequately describe the observed $f(RH)$, with low hygroscopic growth observed at RH values near 70%, in the OA-dominated southeastern US For the remainder of this analysis we will use the κ_{ext} parameterization (Eq. 6) to extrapolate the extinction measured at the three discrete RH values to extinction at ambient RH. In the next section we examine the relationship between κ_{ext} determined from fitting the $f(RH)$ values (Eq. 6) and κ_{chem} calculated from particle composition measurements (Eq. 3). These parameters are related but not identical.

Aerosol hygroscopicity in the southeastern US

C. A. Brock et al.

Title Page

Abstract | Introduction

Conclusions | References

Tables | Figures

◄ | ►

◄ | ►

Back | Close

Full Screen / Esc

Printer-friendly Version

Interactive Discussion

3.2 Relationship between κ_{chem} and κ_{ext}

Equations (2) and (6), which define κ_{chem} and κ_{ext}, are of similar form, but the $f(RH)$ term in Eq. (6) incorporates aerosol extinction, which is a complex function of the particle size distribution and refractive index (Fig. 5). We use a size distribution and Mie scattering model to examine the relationship between κ_{chem} and κ_{ext}. The aerosol was represented as a single-mode lognormal size distribution with a fixed geometric standard deviation of 1.5; the observed interdecile range for the data analyzed here was 1.42–1.60. The geometric mean diameter was varied from 0.04 to 0.5 μm and the κ_{chem} value was varied from 0 to 1. The dry refractive index was fixed at $1.53 + 0i$. At each geometric mean diameter and each value of κ_{chem}, the water uptake was determined at 10, 70, and 90 % RH, which approximately matched the measurement RH values for the low, medium and high CRDS channels, and the extinction from the deliquesced size distribution was calculated. After determining the extinction at all three RH levels, Eq. (6) was fitted to the calculated $f(RH)$ values to determine κ_{ext}. Thus the chemically derived κ_{chem} could be compared with the optically derived κ_{ext} over a range of median particle diameters and κ_{chem} values. As shown in Fig. 6, the ratio of $\kappa_{ext}/\kappa_{chem}$ varied from < 0.4 to > 2.0 over this range of modal diameters and κ_{chem} values. However, for the range of κ_{chem} values of ∼ 0.1 to ∼ 0.4 and the geometric mean diameter range from ∼ 0.1 to ∼ 0.2, approximately matching the ranges observed in the southeastern US (Cerully et al., 2015), the $\kappa_{ext}/\kappa_{chem}$ ratio generally lies between 0.6 and 1.0. Thus κ_{ext} and κ_{chem} are expected to be roughly equivalent in magnitude, with κ_{ext} tending toward smaller values, and to vary approximately proportionally (i.e., the value of $\kappa_{ext}/\kappa_{chem}$ does not change much with changing κ_{chem}).

The $\kappa_{ext}/\kappa_{chem}$ ratio from the simulation described above can be compared with the same ratio determined from the airborne extinction and aerosol composition measurements, also shown in Fig. 6. The measured mean $\kappa_{ext}/\kappa_{chem}$ was 0.52, with considerable dispersion. This ratio is lower than that expected from the simple single-mode lognormal model. This difference may arise because the atmospheric size distribution

Title Page

Abstract | Introduction

Conclusions | References

Tables | Figures

⏮ | ⏭

◀ | ▶

Back | Close

Full Screen / Esc

Printer-friendly Version

Interactive Discussion

is not purely lognormal, and the magnitude of the modeled $\kappa_{ext}/\kappa_{chem}$ shown in Fig. 6 (i.e., the color scale) is sensitive to the assumed geometric standard deviation (although the overall shape of the pattern is not). Over the course of the measurements, κ_{ext} and κ_{chem} were correlated (Fig. 7). The relationships were more linear and with less dispersion for individual flights than for the dataset as a whole, suggesting day-to-day variability in mean size distribution, composition, and/or instrument performance. These data emphasize that κ_{ext} and κ_{chem} are related but substantially different parameters, coupled nonlinearly by Mie theory and the particle size distribution function, and cannot be substituted directly for one another.

3.3 Constraints on the hygroscopicity of OA

Organic aerosol dominated the composition of the submicron particles during both SENEX and SEAC^{4}RS (e.g., Fig. 2a), averaging 65 % of the fine aerosol mass in the data analyzed here. Published values for the hygroscopic growth parameter of OA, $\kappa_{chem,\ OA}$, vary widely between $\sim 0 < \kappa_{chem,\ OA} < 0.4$ (e.g., Petters and Kreidenweiss, 2007; Rickards et al., 2013; Suda et al., 2012). A parameterization linking $\kappa_{chem,\ OA}$ to the ratio of the oxidized OA fragment m/z 44 to total OA mass (f44) as measured in the AMS has been developed (Duplissy et al., 2011). However, Rickards et al. (2013) find that this parameterization does not fit many available data, and that significant variations in aerosol chemical functionality, composition, and oxidation history affect $\kappa_{chem,\ OA}$. Cerully et al. (2015) show that, in the southeastern US, $\kappa_{chem,\ OA}$ is not simply related to oxidation state, but to additional parameters including OA volatility. Values of κ_{chem} for atmospheric aerosols are commonly determined experimentally using measurements of droplet activation diameter in the supersaturated regime (e.g., Cerully et al., 2015; Chang et al., 2010; Dusek et al., 2010; Gunthe et al., 2009; Levin et al., 2012; Sihto et al., 2011) or using hygroscopic growth measurements in the subsaturated regime (Cheung et al., 2015; Hersey et al., 2013; Malm et al., 2000; Mikhailov, 2013; Nguyen et al., 2014; Sihto et al., 2011). Atmospheric variability in these measurements is compounded by potential measurement artifacts (Good et al.,

2010b). Although not always explicitly calculated, the value of $\kappa_{\text{chem, OA}}$ often can be inferred from these studies. A review of results from the publications cited above suggests a range of mass-weighted total $\kappa_{\text{chem,OA}}$ from 0 to 0.2 represents the organic hygroscopicity of the ambient aerosol well in a variety of environments, with best estimates of < 0.1 for subsaturated measurements and > 0.1 for supersaturated measurements. Consistent with these measurements, we use a fixed value of κ_{chem} = 0.085 from Good et al. (2010a) for the water-soluble fraction of OA, which approximately matches observed $f(\text{RH})$ for our data. We further assume that the water soluble fraction of the total OA is 89%, based on measurements made at the Southern Oxidant and Aerosol Study (SOAS) surface site at Centreville, Alabama during the SENEX time frame (Washenfelder et al., 2015). The non-water soluble fraction is assumed to have κ_{chem} = 0, yielding the mass-weighted $\kappa_{\text{chem, OA}}$ of 0.076 in Table 1.

It is possible that the combined measurement uncertainties are sufficiently large that higher values of $\kappa_{\text{chem, OA}}$ might be consistent with our measurements. The relative errors in the calculated extinction at the three RH values (±34%, Sect. 2.4) are not independent and should cancel when calculating $f(\text{RH})$. Ignoring the error terms that cancel, relative errors in calculated $f(\text{RH})_{70}$ of ±7% and in $f(\text{RH})_{90}$ of ±24% were determined using the Monte Carlo method described in Sect. 2.4. To calculate the range in $\kappa_{\text{chem,OA}}$ that was consistent with the observed $f(\text{RH})_{70}$ and $f(\text{RH})_{90}$, the following approach was used: (1) For each measurement point, the inorganic $\kappa_{\text{chem}}r$ determined from the AMS measurements was held constant. (2) A Monte Carlo simulation assigned a random $\kappa_{\text{chem, org}}$ between 0.0 and 0.5, and the values of $f(\text{RH})_{70}$ and $f(\text{RH})_{90}$ were calculated. (3) When the calculated $f(\text{RH})_{70}$ and $f(\text{RH})_{90}$ both agreed with the measured values within their uncertainties, the value of $\kappa_{\text{chem, OA}}$ was recorded; otherwise step (2) was repeated. This process was repeated 50 times for each data point, and the mean value of each $\kappa_{\text{chem, OA}}$ that was consistent with the data was recorded. Thus statistics were built for the values of $\kappa_{\text{chem, OA}}$ that were consistent with observed hygroscopic growth at both the high and medium RH conditions.

Title Page

Abstract	Introduction
Conclusions	References
Tables	Figures

|◀ | ▶|

◀ | ▶

Back | Close

Full Screen / Esc

Printer-friendly Version

Interactive Discussion

A histogram of the values of mean $\kappa_{chem,\,OA}$ that were consistent with the $f(RH)$ observations within uncertainty (Fig. 8) is heavily skewed toward zero, with the 50th, 75th, and 90th percentile values being 0.05, 0.10, and 0.17. This outcome demonstrates that a low value of $\kappa_{chem,\,OA}$ is necessary to match the observed $f(RH)$ values. In particular, only values of $\kappa_{chem,\,OA} < 0.10$ can be consistent with the relatively small increase in $f(RH)$ at the medium RH value of 70 % (Fig. 4a) in most of our data. Our analysis assumes a homogeneous, size-independent internal mixture of the aerosol components, and does not account for the possible presence of sparingly soluble OA compounds (Wex et al., 2009) or for the diameter dependence of κ_{chem} (Good et al., 2010a). Nguyen et al. (2014, Supplement) suggest that κ_{chem} itself is a function of RH due to an increasing osmotic coefficient with decreasing RH. In contrast, we find that a single, constant κ_{chem} explains the $f(RH)$ at both 70 and 90 % RH, but only if $\kappa_{chem,\,OA}$ is < 0.10 for > 75 % of our data.

3.4 Comparison of airborne and ground-based data

The airborne data can be compared with contemporaneous measurements at the SOAS ground site in Centreville of the change in σ_{ext} at wavelengths of 360–420 nm at two RH values (Attwood et al., 2014). Wagner et al. (2015) show that the airborne data measured in the well-mixed afternoon boundary layer over the Centreville site agree well with the surface measurements. Attwood et al. (2014) fit the ground site data using the gamma parameterization (Eq. 1) and find a decrease in hygroscopicity with increasing OA mass fraction that is consistent with earlier studies in different aerosol types. Using the $f(RH)$ measurements by Attwood et al. and solving Eq. (6), κ_{ext} can be calculated and compared with the airborne data. These values are plotted in Fig. 9 against the fraction of the total submicron non-refractory OA mass (note that this differs slightly from the F_{oa} parameter reported by Attwood et al., 2014), as measured by a HR-TOF-AMS at the Centreville site (Xu et al., 2015b). Also plotted are the values from the airborne data used in this analysis, restricted to AMS mass concentrations $> 8\,\mu g\,m^{-3}$ to compare boundary layer air only. The airborne and ground data are

similar, with slopes of -0.24 ± 0.01 and -0.24 ± 0.04, respectively (95 % confidence intervals). The κ_{ext} values from the ground site are higher; however, the κ_{ext} determined from a two-point $f(RH)$ measurement is sensitive to the accuracy of the RH measurements in the extinction cell, as shown by the dashed lines in Fig. 9, which represent the variation in κ_{ext} due to the stated absolute uncertainty in the RH measurement at the ground site of ± 3 %. Extrapolating the central fits to an OA fraction of 1 yields a κ_{ext} of 0.030 for the airborne data and 0.067 for the data from the ground site. Recalling that the ratio of κ_{ext} to κ_{chem} is expected to be ~ 0.5 to 1 for typical accumulation-mode size distributions (Fig. 6), a value of $\kappa_{chem,\,OA}$ of ~ 0.07–0.14 would be expected at the SOAS ground site. These values are approximately consistent with the airborne results showing a relatively low value of $\kappa_{chem,\,OA}$ (< 0.10 for 75 % of the data).

4   Conclusions

The submicron aerosol observed in typical summertime, fair-weather, afternoon conditions in the southeastern US was dominated by OA and displayed a modest increase in extinction with increasing humidity, $f(RH)$. The γ power-law parameterization, which is widely used to describe $f(RH)$ for atmospheric aerosols, did not effectively replicate the observations in this environment, primarily because actual hygroscopic growth was lower than parameterized growth at 70 % RH. An alternative parameterization based on κ-Köhler theory that better describes the observed $f(RH)$ in the southeastern US in summer was developed. This single-parameter κ_{ext} approximation is physically based, yet we caution that it also may not accurately describe $f(RH)$ in many circumstances. For example, the abrupt phase transitions of inorganic salts sometimes observed in the atmosphere (e.g., Santarpia et al., 2005) clearly cannot be described by this smooth function (nor by the γ parameterization). More complex, multi-parameter descriptions of aerosol deliquescence and efflorescence (e.g., Kotchenruther et al., 1999; Mikhailov et al., 2013) are underconstrained by our three-point $f(RH)$ deliquescence measurement. Further, the hygroscopic growth of aerosols dominated by larger particles, such

Full Screen / Esc

Printer-friendly Version

Interactive Discussion

as sea-salt, dust, and primary plant materials is unlikely to follow the κ_{ext} parameterization because the mid-visible extinction efficiency for particles larger than 0.6 µm does not monotonically increase (Fig. 5). However, for a broad range of typical aged continental aerosol size distributions and compositions ranging from background to moderately polluted, from the boundary layer to the free troposphere, the κ_{ext} parameterization effectively describes the $f(\mathrm{RH})$ curve for the deliquesced aerosol.

By reconstructing the extinction based on independently measured composition and size distributions, the OA was found to have had a κ-Köhler hygroscopicity coefficient, $\kappa_{chem, org}$, that was < 0.10 for 75 % of the data assuming nearly all of the OA was water soluble. This value is broadly consistent most previous work measuring atmospheric aerosol hygroscopicity in the subsaturated regime. Many chemistry-climate models use κ-Köhler theory to predict the hygroscopic growth and ambient radiative properties of the aerosol (e.g., Liu et al., 2012). Because OA is a substantial component of the aerosol in many environments (Zhang et al., 2007), it should be a priority to use atmospheric measurements to continue to improve understanding of the factors that control OA hygroscopicity.

References

Attwood, A. R., Washenfelder, R. A., Brock, C. A., Hu, W., Baumann, K., Campuzano-Jost, P., Day, D. A., Edgerton, E. S., Murphy, D. M., Palm, B. B., McComiskey, A., Wagner, N. L., Sá, S. S., Ortega, A., Martin, S. T., Jimenez, J. L., and Brown, S. S.: Trends in sulfate and organic aerosol mass in the Southeast US: impact on aerosol optical depth and radiative forcing, Geophys. Res. Lett., 41, 7701–7709, doi:10.1002/2014GL061669, 2014.

Bahreini, R., Dunlea, E. J., Matthew, B. M., Simons, C., Docherty, K. S., DeCarlo, P. F., Jimenez, J. L., Brock, C. A., and Middlebrook, A. M.: Design and operation of a pressure-controlled inlet for airborne sampling with an aerodynamic aerosol lens, Aerosol Sci. Tech., 42, 465–471, doi:10.1080/02786820802178514, 2008.

Bohren, C. F. and Huffman, D. R.: Absorption and Scattering of Light by Small Particles, John Wiley & Sons, New York, USA, 1983.

Boyd, C. M., Sanchez, J., Xu, L., Eugene, A. J., Nah, T., Tuet, W. Y., Guzman, M. I., and Ng, N. L.: Secondary organic aerosol formation from the β-pinene, +NO$_3$ system: effect of humidity and peroxy radical fate, Atmos. Chem. Phys., 15, 7497–7522, doi:10.5194/acp-15-7497-2015, 2015.

Brock, C. A., Cozic, J., Bahreini, R., Froyd, K. D., Middlebrook, A. M., McComiskey, A., Brioude, J., Cooper, O. R., Stohl, A., Aikin, K. C., de Gouw, J. A., Fahey, D. W., Ferrare, R. A., Gao, R.-S., Gore, W., Holloway, J. S., Hübler, G., Jefferson, A., Lack, D. A., Lance, S., Moore, R. H., Murphy, D. M., Nenes, A., Novelli, P. C., Nowak, J. B., Ogren, J. A., Peischl, J., Pierce, R. B., Pilewskie, P., Quinn, P. K., Ryerson, T. B., Schmidt, K. S., Schwarz, J. P., Sodemann, H., Spackman, J. R., Stark, H., Thomson, D. S., Thornberry, T., Veres, P., Watts, L. A., Warneke, C., and Wollny, A. G.: Characteristics, sources, and transport of aerosols measured in spring 2008 during the aerosol, radiation, and cloud processes affecting Arctic Climate (ARCPAC) Project, Atmos. Chem. Phys., 11, 2423–2453, doi:10.5194/acp-11-2423-2011, 2011.

Brock, C. A., Wagner, N. L., Anderson, B. E., Beyersdorf, A., Campuzano-Jost, P., Day, D. A., Diskin, G. S., Gordon, T. D., Jimenez, J. L., Lack, D. L., Liao, J., Markovic, M. Z., Middlebrook, A. M., Perring, A. E., Richardson, M. S., Schwarz, J. P., Welti, A., Ziemba, L. D., and Murphy, D. M.: Aerosol optical properties in the southeastern United States in summer – Part 2: Sensitivity of aerosol optical depth to meteorological and aerosol parameters, Atmos. Chem. Phys. Discuss., in preparation, 2015.

Title Page

Abstract | Introduction

Conclusions | References

Tables | Figures

|◄ | ►|

◄ | ►

Back | Close

Full Screen / Esc

Printer-friendly Version

Interactive Discussion

Cai, Y., Montague, D., and Mooiweer-Bryan, W.: Performance characteristics of the ultra high sensitivity aerosol spectrometer for particles between 55 and 800 nm: laboratory and field studies, J. Aerosol Sci., 39, 759–769, doi:10.1016/j.jaerosci.2008.04.007, 2008.

Canagaratna, M., Jayne, J., Jimenez, J., Allan, J., Alfarra, M., Zhang, Q., Onasch, T. B., Drewnick, F., Coe, H., Middlebrook, A. M., Delia, A., Williams, L. R., Trimborn, A. M., North-way, M. J., DeCarlo, P. F., Kolb, C. E., Davidovits, P., and Worsnop, D. R.: Chemical and microphysical characterization of ambient aerosols with the Aerodyne aerosol mass spectrometer, Mass Spectrom. Rev., 26, 185–222, 2007.

Cerully, K. M., Bougiatioti, A., Hite Jr., J. R., Guo, H., Xu, L., Ng, N. L., Weber, R., and Nenes, A.: On the link between hygroscopicity, volatility, and oxidation state of ambient and water-soluble aerosols in the southeastern United States, Atmos. Chem. Phys., 15, 8679–8694, doi:10.5194/acp-15-8679-2015, 2015.

Chang, R. Y.-W., Slowik, J. G., Shantz, N. C., Vlasenko, A., Liggio, J., Sjostedt, S. J., Leaitch, W. R., and Abbatt, J. P. D.: The hygroscopicity parameter (κ) of ambient organic aerosol at a field site subject to biogenic and anthropogenic influences: relationship to degree of aerosol oxidation, Atmos. Chem. Phys., 10, 5047–5064, doi:10.5194/acp-10-5047-2010, 2010.

Charlson, R. J., Horvath, H., and Pueschel, R. F.: The direct measurement of atmospheric light scattering coefficient for studies of visibility and pollution, Atmos. Environ., 1, 469–478, 1967.

Cheung, H. H. Y., Yeung, M. C., Li, Y. J., Lee, B. P., and Chan, C. K.: Relative humidity-dependent HTDMA measurements of ambient aerosols at the HKUST supersite in Hong Kong, China, Aerosol Sci. Tech., 49, 643–654, doi:10.1080/02786826.2015.1058482, 2015.

Chylek, P.: Extinction and liquid water content of fogs and clouds, J. Atmos. Sci., 35, 296–300, 1978.

Covert, D. S. and Charlson, R. J.: A study of the relationship of chemical composition and humidity to light scattering by aerosols, J. Appl. Meteorol., 11, 968–976, 1972.

Day, D. A., Campuzano-Jost, P., Palm, B. B., Hu, W., Nault, B. A., Wooldridge, P. J., Cohen, R. C., Docherty, K. S., Wagner, N. L., and Jimenez, J. L.: Observations of particle organic nitrate from airborne and ground platforms in North America: insights into vertical and geographical distributions, gas/particle partitioning, losses, and contributions to total particle nitrate, in preparation, 2015.

Title Page

Abstract | Introduction

Conclusions | References

Tables | Figures

|◄ | ►|

◄ | ►

Back | Close

Full Screen / Esc

Printer-friendly Version

Interactive Discussion

DeCarlo, P. F., Kimmel, J. R., Trimborn, A., Northway, M. J., Jayne, J. T., Aiken, A. C., Gonin, M., Fuhrer, K., Horvath, T., Docherty, K. S., Worsnop, D. R., and Jimenez, J. L.: Field-deployable, high-resolution, time-of-flight aerosol mass spectrometer, Anal. Chem., 78, 8281–8289, doi:10.1021/ac061249n, 2006.

Doherty, J. P. K. Quinn, S., Jefferson, A., Carrico, C. M., Anderson, T. L., and Hegg., D.: A comparison and summary of aerosol optical properties as observed in situ from aircraft, ship, and land during ACE-Asia, J. Geophys. Res., 110, D04201, doi:10.1029/2004JD004964, 2005.

Draper, D. C., Farmer, D. K., Desyaterik, Y., and Fry, J. L.: A comparison of secondary organic aerosol (SOA) yields and composition from ozonolysis of monoterpenes at varying concentrations of NO_2, Atmos. Chem. Phys. Discuss., 15, 14923–14960, doi:10.5194/acpd-15-14923-2015, 2015.

Dunlea, E. J., DeCarlo, P. F., Aiken, A. C., Kimmel, J. R., Peltier, R. E., Weber, R. J., Tomlinson, J., Collins, D. R., Shinozuka, Y., McNaughton, C. S., Howell, S. G., Clarke, A. D., Emmons, L. K., Apel, E. C., Pfister, G. G., van Donkelaar, A., Martin, R. V., Millet, D. B., Heald, C. L., and Jimenez, J. L.: Evolution of Asian aerosols during transpacific transport in INTEX-B, Atmos. Chem. Phys., 9, 7257–7287, doi:10.5194/acp-9-7257-2009, 2009.

Duplissy, J., DeCarlo, P. F., Dommen, J., Alfarra, M. R., Metzger, A., Barmpadimos, I., Prevot, A. S. H., Weingartner, E., Tritscher, T., Gysel, M., Aiken, A. C., Jimenez, J. L., Canagaratna, M. R., Worsnop, D. R., Collins, D. R., Tomlinson, J., and Baltensperger, U.: Relating hygroscopicity and composition of organic aerosol particulate matter, Atmos. Chem. Phys., 11, 1155–1165, doi:10.5194/acp-11-1155-2011, 2011.

Dusek, U., Frank, G. P., Curtius, J., Drewnick, F., Schneider, J., Kürten, A., Rose, D., Andreae, M. O., Borrmann, S., and Pöschl, U.: Enhanced organic mass fraction and decreased hygroscopicity of cloud condensation nuclei (CCN) during new particle formation events, Geophys. Res. Lett., 37, L03804, doi:10.1029/2009GL040930, 2010.

Friedlander, S. K. and Wang, C. S.: The self-preserving particle size distribution for coagulation by Brownian motion, J. Colloid Interf. Sci., 22, 126–132, doi:10.1016/0021-9797(66)90073-7, 1966.

Fry, J. L., Kiendler-Scharr, A., Rollins, A. W., Wooldridge, P. J., Brown, S. S., Fuchs, H., Dubé, W., Mensah, A., dal Maso, M., Tillmann, R., Dorn, H.-P., Brauers, T., and Cohen, R. C.: Organic nitrate and secondary organic aerosol yield from NO_3 oxidation of β-pinene evaluated using a gas-phase kinetics/aerosol partitioning model, Atmos. Chem. Phys., 9, 1431–1449, doi:10.5194/acp-9-1431-2009, 2009.

Title Page

Abstract | Introduction

Conclusions | References

Tables | Figures

Back | Close

Full Screen / Esc

Printer-friendly Version

Interactive Discussion

Good, N., Topping, D. O., Allan, J. D., Flynn, M., Fuentes, E., Irwin, M., Williams, P. I., Coe, H., and McFiggans, G.: Consistency between parameterisations of aerosol hygroscopicity and CCN activity during the RHaMBLe discovery cruise, Atmos. Chem. Phys., 10, 3189–3203, doi:10.5194/acp-10-3189-2010, 2010a.

Good, N., Topping, D. O., Duplissy, J., Gysel, M., Meyer, N. K., Metzger, A., Turner, S. F., Baltensperger, U., Ristovski, Z., Weingartner, E., Coe, H., and McFiggans, G.: Widening the gap between measurement and modelling of secondary organic aerosol properties?, Atmos. Chem. Phys., 10, 2577–2593, doi:10.5194/acp-10-2577-2010, 2010b.

Gunthe, S. S., King, S. M., Rose, D., Chen, Q., Roldin, P., Farmer, D. K., Jimenez, J. L., Artaxo, P., Andreae, M. O., Martin, S. T., and Pöschl, U.: Cloud condensation nuclei in pristine tropical rainforest air of Amazonia: size-resolved measurements and modeling of atmospheric aerosol composition and CCN activity, Atmos. Chem. Phys., 9, 7551–7575, doi:10.5194/acp-9-7551-2009, 2009.

Hale, G. M. and Querry, M. R.: Optical constants of water in the 200-nm to 200-µm wavelength region, Appl. Optics, 12, 555–563, 1973.

Hand, J. L. and Kreidenweis, S. M.: A new method for retrieving particle refractive index and effective density from aerosol size distribution data, Aerosol Sci. Tech., 36, 1012–1026, doi:10.1080/02786820290092276, 2002.

Hänel, G.: Computation of the extinction of visible radiation by atmospheric aerosol particles as a function of the relative humidity, based upon measured properties, J. Aerosol Sci., 3, 377–386, doi:10.1016/0021-8502(72)90092-4, 1972a.

Hänel, G.: The ratio of the extinction coefficient to the mass of atmospheric aerosol particles as a function of the relative humidity, J. Aerosol Sci., 3, 455–460, doi:10.1016/0021-8502(72)90075-4, 1972b.

Hänel, G.: Single-scattering albedo of atmospheric aerosol particles as a function of relative humidity, J. Atmos. Sci., 33, 1120–1124, 1976.

Haynes, W. M., Lide, D. R., and Bruno, T. J.: CRC Handbook of Chemistry and Physics: a Ready-Reference Book of Chemical and Physical Data, CRC Press, Boca Raton, FL, US, 2014.

Hegg, D., Larson, T., and Yuen, P. F.: A theoretical study of the effect of relative humidity on light scattering by tropospheric aerosols, J. Geophys. Res., 98, 18435–18439, 1993.

Hersey, S. P., Craven, J. S., Metcalf, A. R., Lin, J., Lathem, T., Suski, K. J., Cahill, J. F., Duong, H. T., Sorooshian, A., Jonsson, H. H., Shiraiwa, M., Zuend, A., Nenes, A.,

Prather, K. A., Flagan, R. C., and Seinfeld, J. H.: Composition and hygroscopicity of the Los Angeles Aerosol: CalNex, J. Geophys. Res., 118, 3016–3036, doi:10.1002/jgrd.50307, 2013.

Hodas, N., Zuend, A., Mui, W., Flagan, R. C., and Seinfeld, J. H.: Influence of particle-phase state on the hygroscopic behavior of mixed organic–inorganic aerosols, Atmos. Chem. Phys., 15, 5027–5045, doi:10.5194/acp-15-5027-2015, 2015.

IPCC, Stocker, T. F., Qin, D., Plattner, G.-K., Tignor, M., Allen, S. K., Boschung, J., Nauels, A., Xia, Y., Bex, V., and Midgley, P. M. (Eds.): Climate Change 2013: The Physical Science Basis. Contribution of Working Group I to the Fifth Assessment Report of the Intergovernmental Panel on Climate Change. Cambridge University Press, Cambridge, UK, New York, NY, USA, doi:10.1017/CBO9781107415324, 2013.

Kasten, F.: Visibility forecast in the phase of pre-condensation, Tellus, 21, 631–635, 1969.

Kotchenruther, R. A., Hobbs, P. V., and Hegg, D. A.: Humidification factors for atmospheric aerosols off the mid-Atlantic coast of the United States, J. Geophys. Res., 104, 2239–2251, 1999.

Langridge, J. M., Richardson, M. S., Lack, D., Law, D., and Murphy, D. M.: Aircraft instrument for comprehensive characterization of aerosol optical properties, Part I: Wavelength-dependent optical extinction and its relative humidity dependence measured using cavity ringdown spectroscopy, Aerosol Sci. Tech., 45, 1305–1318, doi:10.1080/02786826.2011.592745, 2011.

Levin, E. J. T., Prenni, A. J., Petters, M. D., Kreidenweis, S. M., Sullivan, R. C., Atwood, S. A., Ortega, J., DeMott, P. J., and Smith, J. N.: An annual cycle of size-resolved aerosol hygroscopicity at a forested site in Colorado, J. Geophys. Res., 117, D06201, doi:10.1029/2011JD016854, 2012.

Liao, J., Froyd, K. D., Murphy, D. M., Keutsch, F. N., Yu, G., Wennberg, P. O., St. Clair, J. M., Crounse, J. D., Wisthaler, A., Mikoviny, T., Jimenez, J. L, Campuzano-Jost, P., Day, D. A., Hu, W., Ryerson, T. B., Pollack, I. B., Peischl, J., Anderson, B. E., Ziemba, L. D., Blake, D. R., Meinardi, S., and Diskin, G.: Airborne measurements of organosulfates over the continental US, J. Geophys. Res., 120, 2990–3005, doi:10.1002/2014JD022378, 2015.

Liu, X., Easter, R. C., Ghan, S. J., Zaveri, R., Rasch, P., Shi, X., Lamarque, J.-F., Gettelman, A., Morrison, H., Vitt, F., Conley, A., Park, S., Neale, R., Hannay, C., Ekman, A. M. L., Hess, P., Mahowald, N., Collins, W., Iacono, M. J., Bretherton, C. S., Flanner, M. G., and Mitchell, D.: Toward a minimal representation of aerosols in climate models: description and

Title Page

Abstract | Introduction

Conclusions | References

Tables | Figures

|◄ | ►|

◄ | ►

Back | Close

Full Screen / Esc

Printer-friendly Version

Interactive Discussion

Title Page

Abstract | Introduction

Conclusions | References

Tables | Figures

|◀ | ▶|

◀ | ▶

Back | Close

Full Screen / Esc

Printer-friendly Version

Interactive Discussion

evaluation in the Community Atmosphere Model CAM5, Geosci. Model Dev., 5, 709–739, doi:10.5194/gmd-5-709-2012, 2012.

Malm, W. C., Day, D. E., and Kreidenweis, S. M.: Light scattering characteristics of aerosols as a function of relative humidity: Part I – a comparison of measured scattering and aerosol concentrations using the theoretical models, J. Air Waste Manage., 50, 686–700, doi:10.1080/10473289.2000.10464117, 2000.

Massoli, P., Bates, T., Quinn, P., and Lack, D.: Aerosol optical and hygroscopic properties during TexAQS-GoMACCS 2006 and their impact on aerosol direct radiative forcing, J. Geophys. Res., 114, D00F07, doi:10.1029/2008JD011604, 2009.

Middlebrook, A. M., Bahreini, R., Jimenez, J. L., and Canagaratna, M. R.: Evaluation of composition-dependent collection efficiencies for the Aerodyne aerosol mass spectrometer using field data, Aerosol Sci. Tech., 46, 258–271, doi:10.1080/02786826.2011.620041, 2012.

Mikhailov, E., Vlasenko, S., Rose, D., and Pöschl, U.: Mass-based hygroscopicity parameter interaction model and measurement of atmospheric aerosol water uptake, Atmos. Chem. Phys., 13, 717–740, doi:10.5194/acp-13-717-2013, 2013.

Nguyen, T. K. V., Petters, M. D., Suda, S. R., Guo, H., Weber, R. J., and Carlton, A. G.: Trends in particle-phase liquid water during the Southern Oxidant and Aerosol Study, Atmos. Chem. Phys., 14, 10911–10930, doi:10.5194/acp-14-10911-2014, 2014.

Petters, M. D. and Kreidenweis, S. M.: A single parameter representation of hygroscopic growth and cloud condensation nucleus activity, Atmos. Chem. Phys., 7, 1961–1971, doi:10.5194/acp-7-1961-2007, 2007.

Petzold, A., Formenti, P., Baumgardner, D., Bundke, U., Coe, H., Curtius, J., DeMott, P. J., Flagan, R. C., Fiebig, M., Hudson, J. G., McQuaid, J., Minikin, A., Roberts, G. C., and Wang, J.: In situ measurements of aerosol particles, in: Airborne Measurements for Environmental Research: Methods and Instruments, J. Wiley & Sons, New York, USA, ISBN: 978-3-527-40996-9, 157–224, 2013.

Pilat, M. J. and Charlson, R. J.: Theoretical and optical studies of humidity effects on the size distribution of a hygroscopic aerosol, J. Rech. Atmos., 2, 165–170, 1966.

Pinnick, R. G., Jennings, S. G., and Chýlek, P.: Relationships between extinction, absorption, backscattering, and mass content of sulfuric acid aerosols, J. Geophys. Res., 85, 4059–4066, 1980.

Pringle, K. J., Tost, H., Pozzer, A., Pöschl, U., and Lelieveld, J.: Global distribution of the effective aerosol hygroscopicity parameter for CCN activation, Atmos. Chem. Phys., 10, 5241–5255, doi:10.5194/acp-10-5241-2010, 2010.

Quinn, P. K., Bates, T. S., Baynard, T., Clarke, A. D., Onasch, T. B., Wang, W., Rood, M. J., Andrews, E., Allan, J., Carrico, C. M., Coffman, D., and Worsnop, D.: Impact of particulate organic matter on the relative humidity dependence of light scattering: a simplified parameterization, Geophys. Res. Lett., 32, L22809, doi:10.1029/2005GL024322, 2005.

Rickards, A. M. J., Miles, R. E. H., Davies, J. F., Marshall, F. H., and Reid, J. P.: Measurements of the sensitivity of aerosol hygroscopicity and the κ parameter to the O/C ratio, J. Phys. Chem. A, 117, 14120–14131, doi:10.1021/jp407991n, 2013.

Rissler, J., Vestin, A., Swietlicki, E., Fisch, G., Zhou, J., Artaxo, P., and Andreae, M. O.: Size distribution and hygroscopic properties of aerosol particles from dry-season biomass burning in Amazonia, Atmos. Chem. Phys., 6, 471–491, doi:10.5194/acp-6-471-2006, 2006.

Santarpia, J. L., Gasparini, R., Li, R., and Collins, D. R.: Diurnal variations in the hygroscopic growth cycles of ambient aerosol populations, J. Geophys. Res., 110, D03206, doi:10.1029/2004JD005279, 2005.

Schwarz, J. P., Perring, A. E., Markovic, M. Z., Gao, R. S., Ohata, S., Langridge, J., Law, D., McLaughlin, R., and Fahey, D. W.; Technique and theoretical approach for quantifying the hygroscopicity of black-carbon-containing aerosol using a single particle soot photometer, J. Aerosol Sci., 81., 110–126, doi:10.1016/j.jaerosci.2014.11.009, 2015.

Sihto, S.-L., Mikkilä, J., Vanhanen, J., Ehn, M., Liao, L., Lehtipalo, K., Aalto, P. P., Duplissy, J., Petäjä, T., Kerminen, V.-M., Boy, M., and Kulmala, M.: Seasonal variation of CCN concentrations and aerosol activation properties in boreal forest, Atmos. Chem. Phys., 11, 13269–13285, doi:10.5194/acp-11-13269-2011, 2011.

Stokes, R. H. and Robinson, R. A.: Interactions in aqueous nonelectrolyte solutions, I. Solute-solvent equilibria, J. Phys. Chem., 70, 2126–2131, doi:10.1021/j100879a010, 1966.

Suda, S. R., Petters, M. D., Matsunaga, A., Sullivan, R. C., Ziemann, P. J., and Kreidenweis, S. M.: Hygroscopicity frequency distributions of secondary organic aerosols, J. Geophys. Res., 117, D04207, doi:10.1029/2011JD016823, 2012.

Tang, I. N.: Chemical and size effects of hygroscopic aerosols on light scattering coefficients, J. Geophys. Res., 101, 19245–19250, 1996.

Title Page

Abstract | Introduction

Conclusions | References

Tables | Figures

|◀ | ▶|

◀ | ▶

Back | Close

Full Screen / Esc

Printer-friendly Version

Interactive Discussion

Toon, O. B., Pollack, J. B., and Khare, B. N.: The optical constants of several atmospheric aerosol species: ammonium sulfate, aluminum oxide, and sodium chloride, J. Geophys. Res., 81, 5733–5748, doi:10.1029/JC081i033p05733, 1976.

Varma, R. M., Ball, S. M., Brauers, T., Dorn, H.-P., Heitmann, U., Jones, R. L., Platt, U., Pöhler, D., Ruth, A. A., Shillings, A. J. L., Thieser, J., Wahner, A., and Venables, D. S.: Light extinction by secondary organic aerosol: an intercomparison of three broadband cavity spectrometers, Atmos. Meas. Tech., 6, 3115–3130, doi:10.5194/amt-6-3115-2013, 2013.

Wagner, N. L., Brock, C. A., Angevine, W. M., Beyersdorf, A., Campuzano-Jost, P., Day, D., de Gouw, J. A., Diskin, G. S., Gordon, T. D., Graus, M. G., Holloway, J. S., Huey, G., Jimenez, J. L., Lack, D. A., Liao, J., Liu, X., Markovic, M. Z., Middlebrook, A. M., Mikoviny, T., Peischl, J., Perring, A. E., Richardson, M. S., Ryerson, T. B., Schwarz, J. P., Warneke, C., Welti, A., Wisthaler, A., Ziemba, L. D., and Murphy, D. M.: In situ vertical profiles of aerosol extinction, mass, and composition over the southeast United States during SENEX and SEAC[4]RS: observations of a modest aerosol enhancement aloft, Atmos. Chem. Phys., 15, 7085–7102, doi:10.5194/acp-15-7085-2015, 2015.

Warren, S. G., Hahn, C. J., London, J., Chervin, R. M., and Jenne, R. L.: Global Distribution of Total Cloud Cover and Cloud Type Amounts over Land, NCAR Tech. Note TN-273_STR, 1–232, available at: http://opensky.library.ucar.edu/collections/TECH-NOTE-000-000-000-628 (last access: 17 September 2015), 1986.

Washenfelder, R. A., Attwood, A. R., Brock, C. A., Guo, H., Xu, L., Weber, R. J., Ng, N. L., Allen, H. M., Ayres, B. R., Baumann, K., Cohen, R. C., Draper, D. C., Duffey, K. C., Edgerton, E., Fry, J. L., Hu, W. W., Jimenez, J. L., Palm, B. B., Romer, P., Stone, E. A., Wooldridge, P. J., and Brown, S. S.: Biomass burning dominates brown carbon absorption in the rural southeastern United States, Geophys. Res. Lett., 42, 653–664, doi:10.1002/2014GL062444, 2015.

Wex, H., Petters, M. D., Carrico, C. M., Hallbauer, E., Massling, A., McMeeking, G. R., Poulain, L., Wu, Z., Kreidenweis, S. M., and Stratmann, F.: Towards closing the gap between hygroscopic growth and activation for secondary organic aerosol: Part 1 – Evidence from measurements, Atmos. Chem. Phys., 9, 3987–3997, doi:10.5194/acp-9-3987-2009, 2009.

Wright, H. L.: Atmospheric opacity: a study of visibility observations in the British Isles, Q. J. Roy. Meteor. Soc., 65, 411–442, 1939.

Xu, L., Guo, H., Boyd, C. M., Klein, M., Bougiatioti, A., Cerully, K. M., Hite, J. R., Isaacman-VanWertz, G., Kreisberg, N. M., Knote, C., Olson, K., Koss, A., Goldstein, A. H., Hering, S. V.,

Title Page

Abstract | Introduction

Conclusions | References

Tables | Figures

|◄ | ►|

◄ | ►

Back | Close

Full Screen / Esc

Printer-friendly Version

Interactive Discussion

de Gouw, J., Baumann, K., Lee, S.-H., Nenes, A., Weber, R. J., and Ng, N. L.: Effects of anthropogenic emissions on aerosol formation from isoprene and monoterpenes in the southeastern United States, P. Natl. Acad. Sci. USA, 112, 37–42, 2015a.

Xu, L., Suresh, S., Guo, H., Weber, R. J., and Ng, N. L.: Aerosol characterization over the southeastern United States using high-resolution aerosol mass spectrometry: spatial and seasonal variation of aerosol composition and sources with a focus on organic nitrates, Atmos. Chem. Phys., 15, 7307–7336, doi:10.5194/acp-15-7307-2015, 2015b.

Zaveri, R. A.: A new method for multicomponent activity coefficients of electrolytes in aqueous atmospheric aerosols, J. Geophys. Res., 110, D02201, doi:10.1029/2004JD004681, 2005.

Zhang, Q., Jimenez, J. L., Canagaratna, M. R., Allan, J. D., Coe, H., Ulbrich, I., Alfarra, M. R., Takami, A., Middlebrook, A. M., Sun, Y. L., Dzepina, K., Dunlea, E., Docherty, K., De-Carlo, P. F., Salcedo, D., Onasch, T., Jayne, J. T., Miyoshi, T., Shimono, A., Hatakeyama, S., Takegawa, N., Kondo, Y., Schneider, J., Drewnick, F., Borrmann, S., Weimer, S., Demerjian, K., Williams, P., Bower, K., Bahreini, R., Cottrell, L., Griffin, R. J., Rautiainen, J., Sun, J. Y., Zhang, Y. M., and Worsnop, D. R.: Ubiquity and dominance of oxygenated species in organic aerosols in anthropogenically-influenced Northern Hemisphere midlatitudes, Geophys. Res. Lett., 34, L13801, doi:10.1029/2007GL029979, 2007.

Table 1. Parameters used to calculate ambient extinction.

Species	Refractive Index	reference	κ_{chem}	reference	Density	reference
H_2O	1.33	Hale and Querry (1973)	N/A	N/A	1.00	N/A
OA	1.48	Varma et al. (2013)	0.076	Good et al. (2010a); Petters and Kreidenweis (2008)[1]	1.4	Hand and Kreidenweis (2002)
H_2SO_4	1.408	Hand and Kreidenweis (2002)	0.870	Good et al. (2010a); Petters and Kreidenweis (2008)	1.8	Hand and Kreidenweis (2002)
$(NH_4)HSO_4$	1.479	Hand and Kreidenweis (2002)	0.543	Good et al. (2010a)	1.78	Hand and Kreidenweis (2002)
$(NH_4)_3H(SO_4)_2$	1.53	Hand and Kreidenweis (2002)	0.579	Good et al. (2010a)	1.83	Hand and Kreidenweis (2002)
$(NH_4)_2SO_4$	1.527	Hand and Kreidenweis (2002)	0.483	Good et al. (2010a)	1.76	Hand and Kreidenweis (2002); Nguyen et al. (2014)
HNO_3	1.393	Haynes et al. (2014)	0.999	Good et al. (2010a)	1.5129	Good et al. (2010); Haynes et al. (2014)
NH_4NO_3	1.553	Tang (1996))	0.597	Good et al. (2010a)	1.725	Tang (1996)
HCl	1.329	Haynes et al. (2014)	0.5	assumed[2]	1.49	Haynes et al. (2014)
NH_4Cl	1.64	Haynes et al. (2014)	0.5	assumed[2]	1.519	Haynes et al. (2014)

[1] Good et al. (2010a) assume κ_{org} = 0.085. We apply this value to the water-soluble fraction of fine OA, which was estimated to be 89 % based on measurements at the SOAS ground site (Washenfelder et al., 2015).

[1] No literature values found. These species contributed negligibly to aerosol mass and hygroscopicity.

Title Page

Abstract | Introduction

Conclusions | References

Tables | Figures

◄ | ►

Back | Close

Full Screen / Esc

Printer-friendly Version

Interactive Discussion

Table 2. Linear regression parameters between calculated extinction and measured extinction at 532 nm and 3 relative humidities for each flight analyzed in this work.

Date	Low RH (< 25%)			Medium RH (~ 70%)			High RH (~ 90%)		
	r^2	slope	intercept	r^2	slope	intercept	r^2	slope	intercept
3 Jun 2013	0.87[a]	1.02[b]	−3.7	0.96	0.87	−3.6	0.97	1.12	−9.5
11 Jun 2013	0.95	0.89	−3.9	0.95					
12 Jun 2013	0.98	0.87	−0.85	0.98	0.87	−2.4	0.97	1.13	−10.5
16 Jun 2013	0.95	0.74	2.0	0.93	0.81	0.87	0.95	0.88	1.5
22 Jun 2013	0.95	0.74	−4.5	0.95	0.87	−6.4	0.97	0.96	−12.5
29 Jun 2013	0.97	0.73	−0.59	0.92	0.92	−1.7	0.96	0.87	−1.2
30 Aug 2013	0.94	1.04	−3.0	0.93	1.05	−2.6	0.93	1.04	1.2
6 Sep 2013[c]	0.65	0.62	1.3	0.62	0.67	1.1	0.60	0.70	5.0

[a] r^2 values calculated from single-sided linear least squares.
[b] Slope and intercept values calculated from orthogonal distance regression.
[c] No UHSAS data available. Calculated using a TSI, Inc. laser aerosol spectrometer with no refractive index correction.

Figure 1. Schematics showing the process of calculating ambient extinction from **(a)** measurements of composition, size distribution, and ambient RH and **(b)** measurements of ambient RH and of extinction at three instrumental RH values.
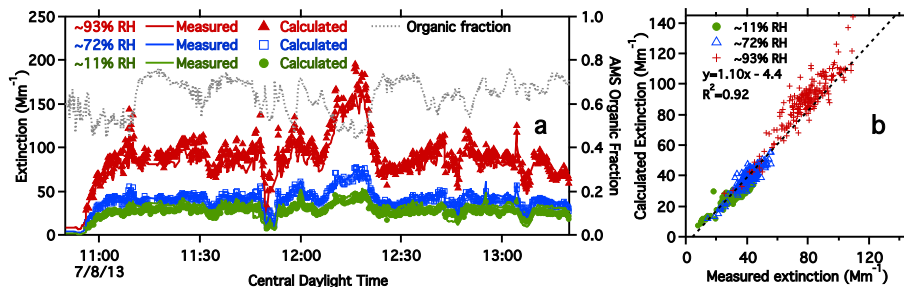
Figure 2. (a) Measured and calculated extinction at three RH values (left axis) and the organic fraction of fine aerosol mass (right axis) measured near local noon on 8 July 2013. **(b)** Calculated vs. measured ambient extinction for all three RH values from **(a)** over the time period from 11:10 and 11:45 LT. Dashed line is a two-sided linear least squares regression.
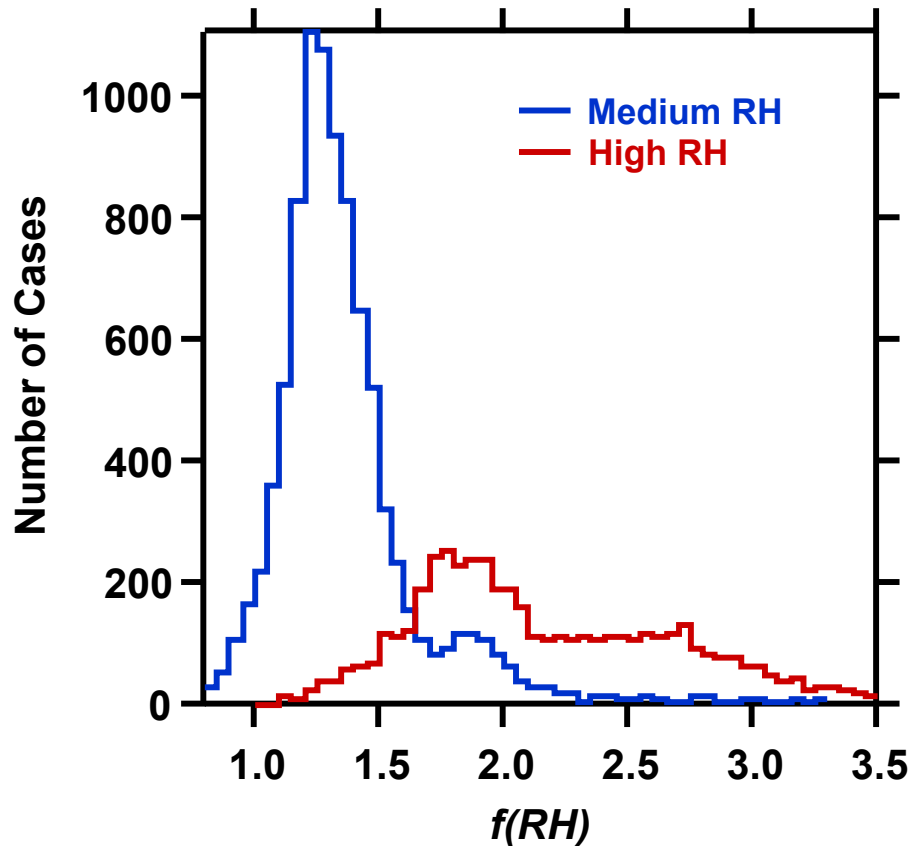
Figure 3. Histograms of values of $f(RH)$ measured at medium RH ($70 \pm 3\%$) and at high RH ($90 \pm 3\%$) for the SENEX and SEAC4RS data selected for this study.
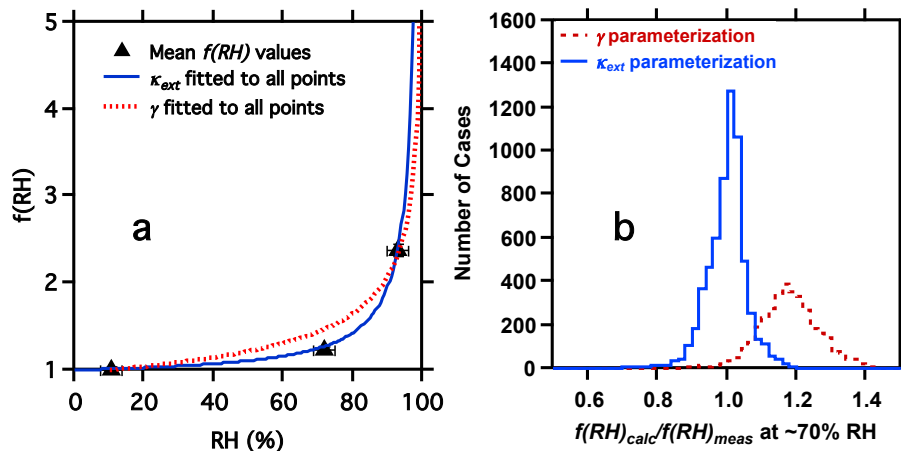
Figure 4. Mean values of $f(RH)$ determined from measurements between 11:10 and 11:45 LT on 8 July 2013 from Fig. 2 (symbols), and curves from the γ power-law parameterization (dashed line, Eq. 1) and the κ_{ext} parameterization (solid line, Eq. 6) fitted to the three data points. Error bars show the standard deviation of the mean values. **(b)** Ratio of calculated to measured $f(RH)$ at $\sim 70\%$ RH for the γ and κ_{ext} parameterizations for all analyzed data.
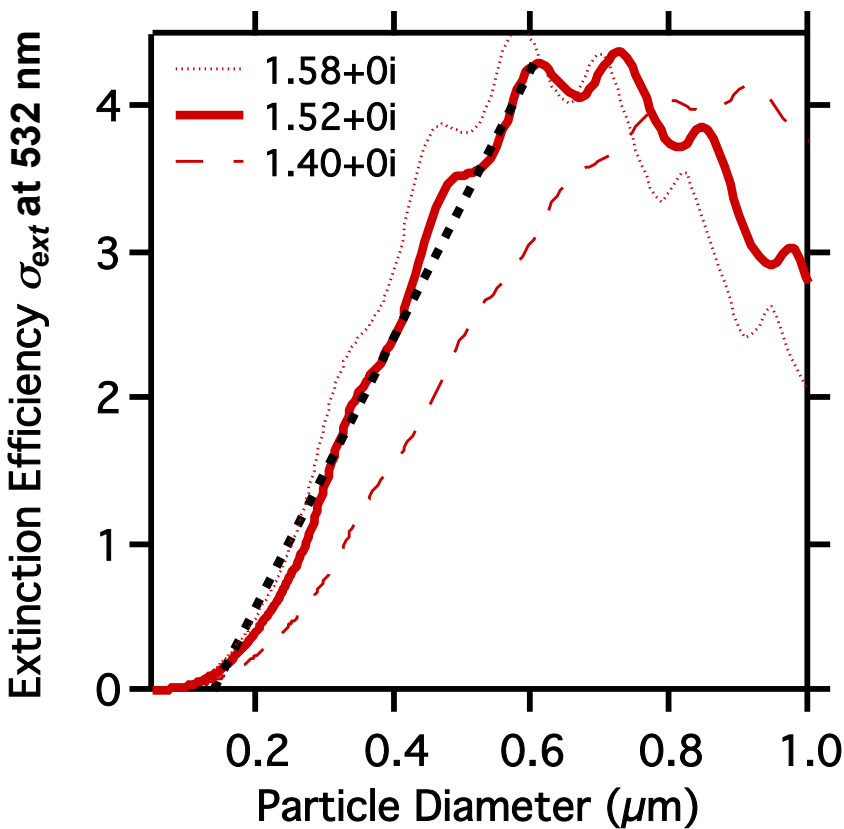
Figure 5. Calculated extinction efficiency for a particle with a refractive index of $1.52 + 0i$ (solid line) and linear least-squares fit for particle diameters between 0.1 and 0.6 μm (dashed line). The extinction efficiency averaged across the size range of hygroscopic growth of a typical accumulation mode aerosol is approximately linear. Extinction efficiency curves for $1.58 + 0i$ and $1.40 + 0i$ are also shown.

Title Page

Abstract | Introduction

Conclusions | References

Tables | Figures

|◀ | ▶|

◀ | ▶

Back | Close

Full Screen / Esc

Printer-friendly Version

Interactive Discussion
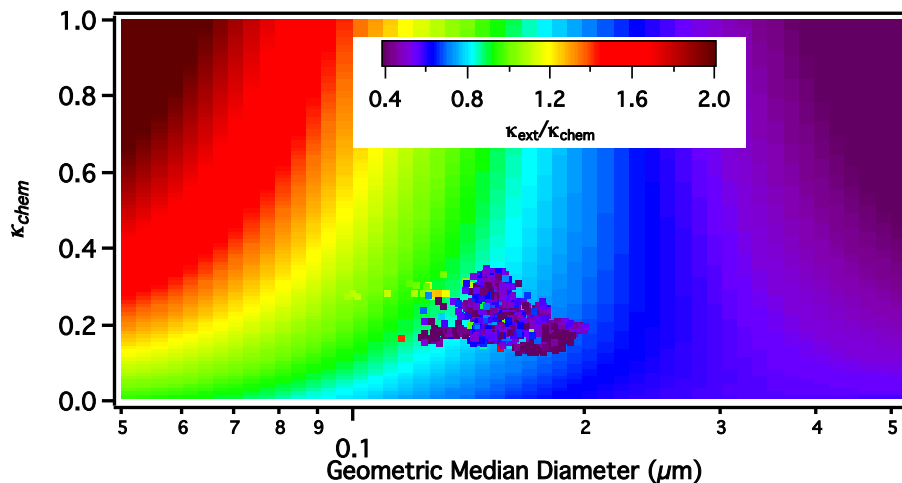
Figure 6. Ratio of optically determined κ_{ext} to chemically determined κ_{chem} as a function of particle geometric median diameter and κ_{chem}. Values of κ_{ext} were calculated for a lognormal particle size distribution with a geometric standard deviation of 1.5 and a geometric median diameter given by the abscissa. Points are instantaneous values of $\kappa_{ext}/\kappa_{chem}$ determined from the in situ $f(\text{RH})$ and composition measurements.

Title Page

Abstract | Introduction

Conclusions | References

Tables | Figures

|◀ | ▶|

◀ | ▶

Back | Close

Full Screen / Esc

Printer-friendly Version

Interactive Discussion
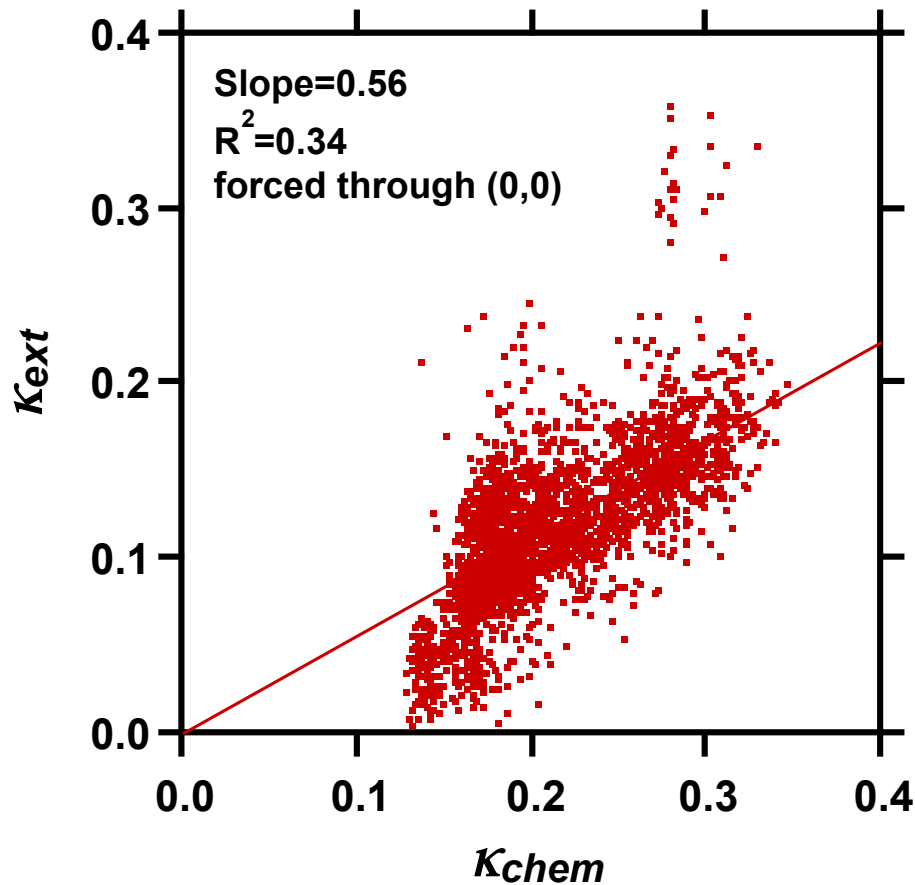
Figure 7. Values of κ_{ext} determined from fitting Eq. (6) to the f(RH) data plotted as a function of κ_{chem} calculated from aerosol composition measurements using κ-Köhler theory (Eq. 3).
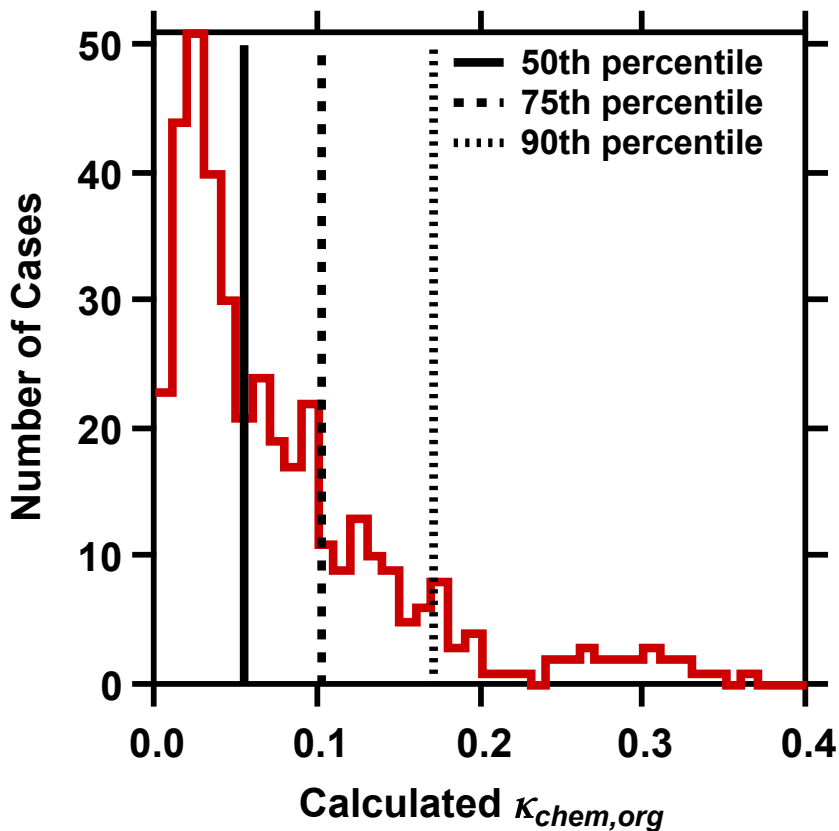
Figure 8. Histogram of results from a Monte Carlo analysis showing values of the organic κ_{chem} that, given the observed inorganic composition and size distribution, are consistent within experimental uncertainty with the measured f(RH). Vertical lines indicate the 50th, 75th, and 90th percentile values of the histogram.

Title Page

Abstract | Introduction

Conclusions | References

Tables | Figures

|◄ | ►|

◄ | ►

Back | Close

Full Screen / Esc

Printer-friendly Version

Interactive Discussion
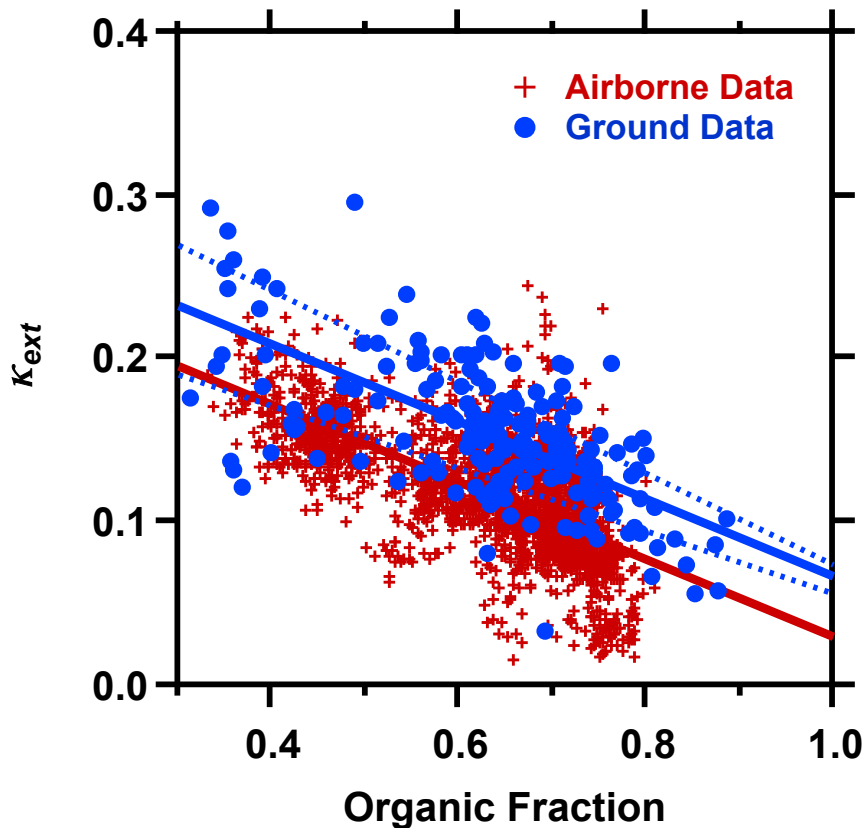
Figure 9. Comparison of κ_{ext} as function of the fraction of sub-0.7 μm non-refractory OA for the data analyzed in this paper (crosses) and similar measurements at the SOAS ground site in Centreville, Alabama, US (Washenfelder et al., 2014) between the hours of 11:00 and 17:00 LT (circles). Dashed lines show regressions to the Centreville data if κ_{ext} is calculated using RH values that vary by the uncertainty of ±3 % RH.

Title Page

Abstract | Introduction

Conclusions | References

Tables | Figures

|◄ | ►|

◄ | ►

Back | Close

Full Screen / Esc

Printer-friendly Version

Interactive Discussion